Electronic Supplementary Material (ESI) for New Journal of Chemistry.
This journal is © The Royal Society of Chemistry and the Centre National de la Recherche Scientifique 2021

Supporting information for

Ultrathin Ti_3C_2 nanosheets served as a high-efficient hole transport layer on Fe_2O_3 photoanode for photoelectrochemical water oxidation

Chenchen Feng[a,b,*], Han Fu[a], Henan Jia[a,b], Haize Jin[a,b], Xiang Cheng[c], Wei Wang[d], Maocheng Liu[a,b,*], Qi Zhou [a,b,*]

[a] *School of Materials Science and Engineering, Lanzhou University of Technology, 287 Langongping Road, Lanzhou 730050, China*

[b] *State Key Laboratory of Advanced Processing and Recycling of Non-ferrous Metals, Lanzhou University of Technology, 287 Langongping Road, Lanzhou 730050, China*

[c] *College of Science, Hebei Agricultural University, Baoding 071001, China*

[d] *State Key Laboratory of High-efficiency Utilization of Coal and Green Chemical Engineering, College of Chemistry and Chemical Engineering, Ningxia University, Yinchuan, 750021, NingXia, China.*

Experimental section

Synthesis of Fe_2O_3 nanorods photoanodes：

3D dendritic Fe_2O_3 nanorods were grown on the acid treated Ti foils. Firstly, untreated Ti foils (1 cm×5 cm) were treated by ultrasonic clean of acetone, ethanol and deionized (DI) water successively. Then, for the HCl treatment, Ti foils were immersed into 30 mL concentrated hydrochloric acid and retained at 80 ℃ for 30 minutes. After that, Ti foils were removed immediately from HCl solution, washed by DI water for several times.

As for the hydrothermal growth of FeOOH nanorods, 1.215 g $FeCl_3 \cdot 6H_2O$ and 0.27 g urea

were dissolved in 60 mL deionized water under vigorous stirring for 30 min. The solution was transferred to a Teflon-lined stainless-steel autoclaves (80 mL), with immersion of a piece of treated Ti foils into the solution. Then the autoclave was sealed and maintained at 100 ℃ for 10 h in an electric oven. After cooled down at room temperature naturally, the prepared Ti foil with FeOOH nanorods cover was taken out. Washed with water and ethanol for numerous times, followed by drying at 60 ℃. Finally, the precursor film was annealed at 550 ℃ in air for 2h. After completing the steps above, the Fe_2O_3 photoanode with dendritic structure was obtained.

Synthesis of Ti_3C_2 nanosheets：

The Ti_3C_2 nanosheets were synthesized according to a previously reported procedure.[1-3] 1.0 g Ti_3AlC_2 power was immersed in 20 mL of 50 wt% HF acid with stirring for 72 h at ice water bath temperature to obtain a stable suspension. The suspension was centrifuged to obtain the solid $Ti_3C_2T_X$ powder, which was then washed several times with DI water until the pH is 7 and dried under vacuum at 60 °C for 12 h. Then, 50 mg of Ti_3C_2 was mixed with 20 mL of dimethyl sulfoxide (DMSO) by stirring for 24 h, followed by centrifugation at 4000 rpm for 20 min to obtain the multilayer $Ti_3C_2T_X$ powders. Then, the precipitate was dispersed in DI water at a mass ratio of 1:300, with argon gas input continuously and sonication for 3 h. After that, the suspension was centrifuged at 4000 rpm for 1 h and the supernatant fluid was collected and dried by freeze drying, named Ti_3C_2 nanosheets.

Synthesis of Fe_2O_3-Ti_3C_2 photoanodes：

The Ti_3C_2 modified Fe_2O_3 photoanodes were prepared by spin-coating Ti_3C_2 dispersed solutions (0.5 mg/mL) at a fixed rotation speed of 600 rpm for 30 seconds and 2000 rpm for 10 seconds on Fe_2O_3 photoanodes. After above, Fe_2O_3-Ti_3C_2 electrodes were heated at 200 °C for 1 h in argon gas, along with the heating rates of 2 ℃/min.

Synthesis of Fe_2O_3-Ti_3C_2-CoAl photoanodes：

CoAl LDH was grown in situ on the Fe_2O_3-Ti_3C_2 photoanodes by hydrothermal method. 0.0437 g $Co(NO_3)_2 \cdot 6H_2O$, 0.0188 g $Al(NO_3)_3 \cdot 9H_2O$, 0.03 g urea, and 0.0074 g NH_4F were dissolved in 10 mL DI water. The solution was then transferred into a 25 mL Teflon-lined stainless-steel autoclave in which a Fe_2O_3-Ti_3C_2 electrode was immersed vertically. The hydrothermal process was taken reaction at 100 °C for 30 min. After being cooled to room temperature naturally, Fe_2O_3-Ti_3C_2-CoAl samples were taken out from the autoclave and rinsed by water and dried at 60 °C for 30 min.

Characterization:

The X-ray diffraction spectra (XRD) measurements were performed on a Rigaku RINT-2000 instrument utilizing Cu Kα radiation (40 KV). The XRD patterns were recorded from 10° to 90° with a scanning rate of 0.067 °/s. Scanning electron microscopy (SEM) measurements were carried out on a field-emission scanning electron microscope (SU8020. HITACHI) operated at an accelerating voltage of 1 KV. Transmission electron microscopy (TEM) measurements were carried out by using a FEI Tecnai TF20 microscope operated at 200 kV. UV-vis diffuse reflectance spectra were taken on an UV-2550 (Shimadzu) spectrometer by using $BaSO_4$ as the reference. The element composition was detected by X-ray photoelectron spectroscope (XPS, ESCALAB 250 Xi, ThermoFisher Scientific), the electron binding energy of the elements measured is corrected based on C 1s of 284.8 eV and matching by peak separation software. Photoluminescence (PL) spectra were monitored by Fluorescence Spectrophotometer (F-7000, Hitachi High-Technologies). All samples were excited with 365 nm light from a pulsed laser.

Photoelectrochemical measurements.

The Photoelectrochemical properties were measured by an electrochemical analyzer (CHI 660D) in a standard three-electrode system with a working electrode, a Pt foil as the counter electrode, and a saturated Ag/AgCl (saturated KCl) as a reference electrode. The photoanodes as the working electrode. The illumination source was a 300 W Xe arc lamp (Beijing Perfectlight Technology Co. Ltd., Microsolar 300 UV) equipped with an AM 1.5G filter, and the power intensity of the incident light was calibrated to 100 mW cm^{-2} at the surface of the working electrode. The linear sweep voltammogram (LSV) curves of the electrodes, with a scan rate of 10 mV s^{-1}. All potentials of the working electrodes were presented against the reversible hydrogen electrode (RHE). The conversion between potentials vs. Ag/AgCl and vs. RHE is performed using the equation below.

$$E_{RHE} = E_{Ag/AgCl} + E_{Ag/AgCl}(reference) + 0.0591 \times pH$$

$$E_{Ag/AgCl}(reference) = 0.1976V\ vs.\ NHE\ at\ 25℃$$

Where pH is a pH value of the electrolyte.

Mott-Schottky measurements were measured in a 1.0 M KOH aqueous solution at a frequency of 1000 Hz and at a scan rate of 50 mV/s. The potential was measured against an Ag/AgCl reference electrode. The donor concentration (N_d) is calculated with the following equation:

$$N_d = \frac{2}{e\varepsilon\varepsilon_0}\left[\frac{d(1/C^2)}{dV}\right]^{-1}$$

Where the electronic charge (e) is 1.6×10^{-19} C, vacuum permittivity (ε_0) is 8.85×10^{-14} F cm^{-1}, the relative permittivity (ε) is 80 for Fe_2O_3, C is the space charge capacitance in the semiconductor (obtained from Mott-Schottky curves), and V is the applied potential.

The incident photon to current efficiency (IPCE) was determined using a solar simulator and monochromator (Beijing NBeT, 71SW 302). IPCE was measured at 1.23 V_{RHE} in 1.0 M KOH solution using the same three-electrode setup described above for photocurrent measurements. IPCE was calculated as follows:

$$IPCE = \frac{1240 \times I(mA/cm^2)}{P_{light}(mW/cm^2) \times \lambda(nm)}$$

Where I is the measured photocurrent density at a specific wavelength, λ is the wavelength of incident light and P_{light} is the measured light power density at that wavelength.

The applied bias photon-to-current efficiency (ABPE) was calculated by following equation:

$$ABPE = \frac{I(mA/cm^2) \times (1.23 - V_{bias})(V)}{P_{light}(mW/cm^2)} \times 100$$

Where I is the photocurrent density from the LSV curves shown in Figure 3A, V_{bias} is the applied bias, P_{light} is the incident illumination power density (100 mW cm^{-2}).

The electrochemical impedance spectroscopy (EIS) Nyquist plots were obtained in a 1.0 M KOH aqueous solution at 1.23 V_{RHE} with small AC amplitude of 10 mV in the frequency range of 10^{-1} to 10^5 Hz under AM 1.5G illumination (100 mW cm^{-2}). The measured spectra were fitted with Z-view software.

Adding 0.5 M H_2O_2 into the 1 M KOH electrolyte can greatly inhibit the recombination of surface charge carriers without affecting the charge separation inside the electrode. The surface charge injection efficiency ($\eta_{injection}$) can be determined as following:

$$\eta_{injection} = J_{H2O}/J_{H2O2}$$

Where J_{H2O} and J_{H2O2} are the photocurrent densities for PEC H_2O oxidation and H_2O_2 oxidation, respectively.

Electrochemical measurements:

Electrolysis experiments were performed in a standard three-electrode cell, which was

composed of working electrode (the as-prepared photoanodes), counter electrode (Pt foil) and reference electrode (Ag/AgCl, sat. KCl). 1 M KOH was used as the electrolyte. The OER properties were performed from 0.1 to 1.5 V vs. Ag/AgCl with a scan rate of 5 mV s^{-1}. The electrochemically active surface areas (ECSAs) were obtained by CV measurement in the non-Faradic region. The range of scanning voltage is -0.38 V - -0.3V (vs. Ag/AgCl), and the scanning rate is 10, 30, 50, 70, 90 and 110 mV S^{-1}. By plotting the $\Delta J = (J_a - J_c)$ at -0.34 V vs. Ag/AgCl against the scan rate, the linear slope which is twice of the double-layer capacitance (C_{dl}) is used to represent ECSAs.

Supplemental Figures and Tables

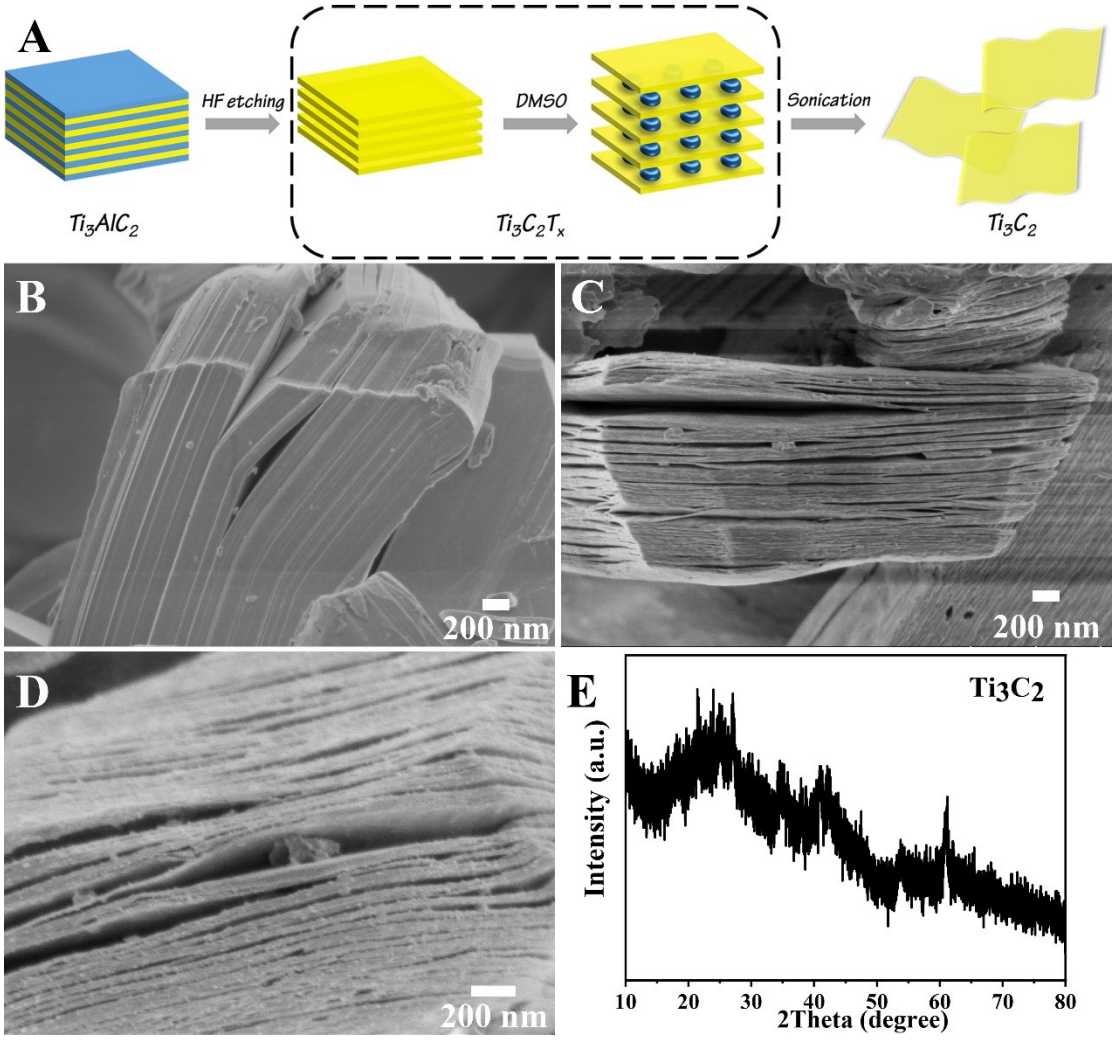

Figure S1. (A) Schematic illustration of the synthetic process of Ti_3C_2. SEM images of Ti_3AlC_2: (B) before and (C)

after HF etching, (D) multilayer $Ti_3C_2T_X$ after DMSO treatment. (E) X-ray diffraction (XRD) spectra of ultrathin Ti_3C_2 nanosheets.

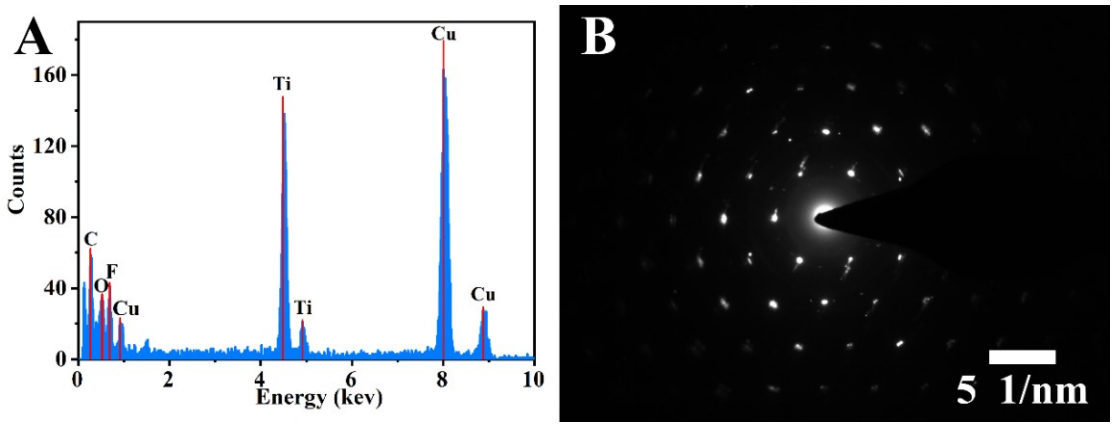

Figure S2. (A) EDX image of the Ti_3C_2 nanosheets. (B) SAED pattern of the interface of the Ti_3C_2 nanosheets.

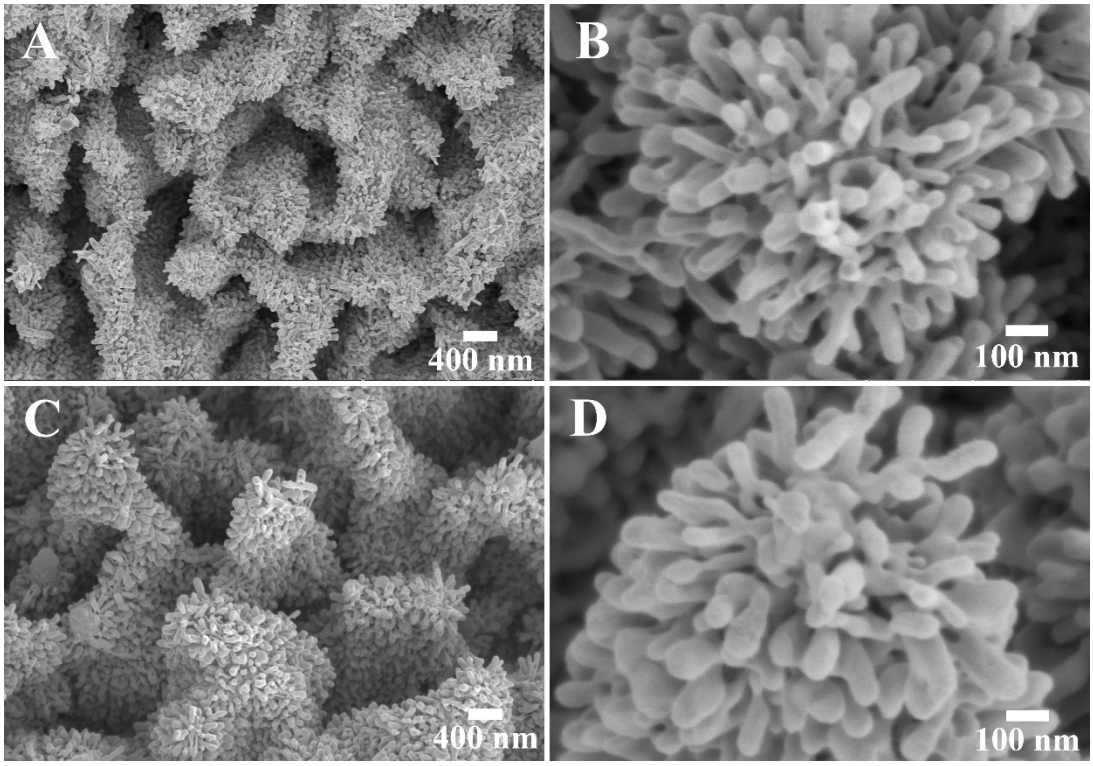

Figure S3. Low and high-resolution SEM morphology characterizations of (A, B) α-Fe_2O_3 and (C, D) Fe_2O_3-Ti_3C_2-CoAl photoanodes.

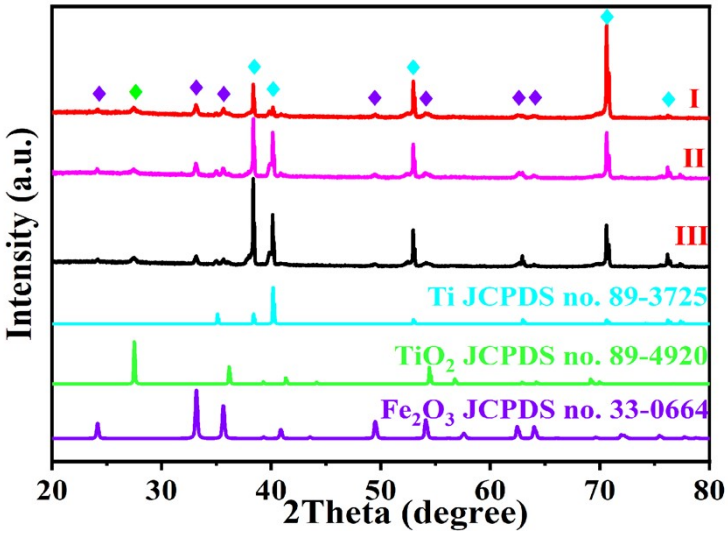

Figure S4. XRD patterns of Fe_2O_3 (III), Fe_2O_3-Ti_3C_2 (II) and Fe_2O_3-Ti_3C_2-CoAl (I) photoanodes.

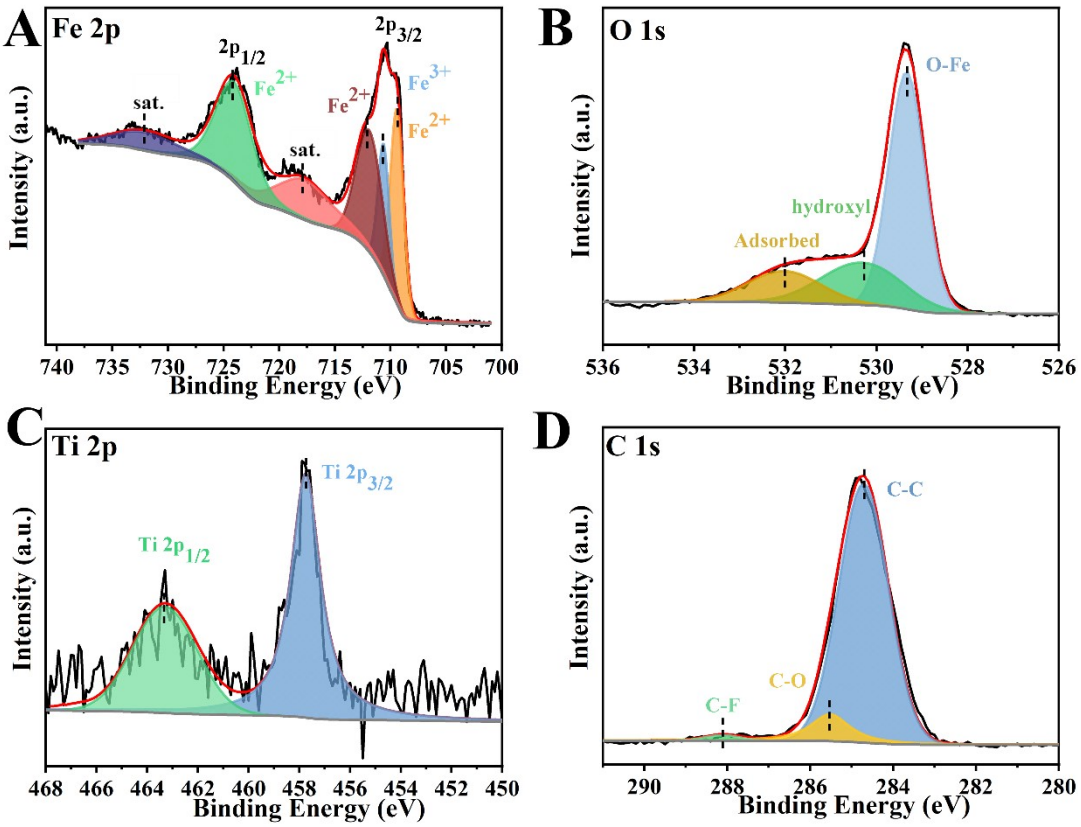

Figure S5. XPS spectra of Fe_2O_3-Ti_3C_2 photoanode. (A) Fe 2p, (B) O 1s, (C) Ti 2p and (D) C 1s.

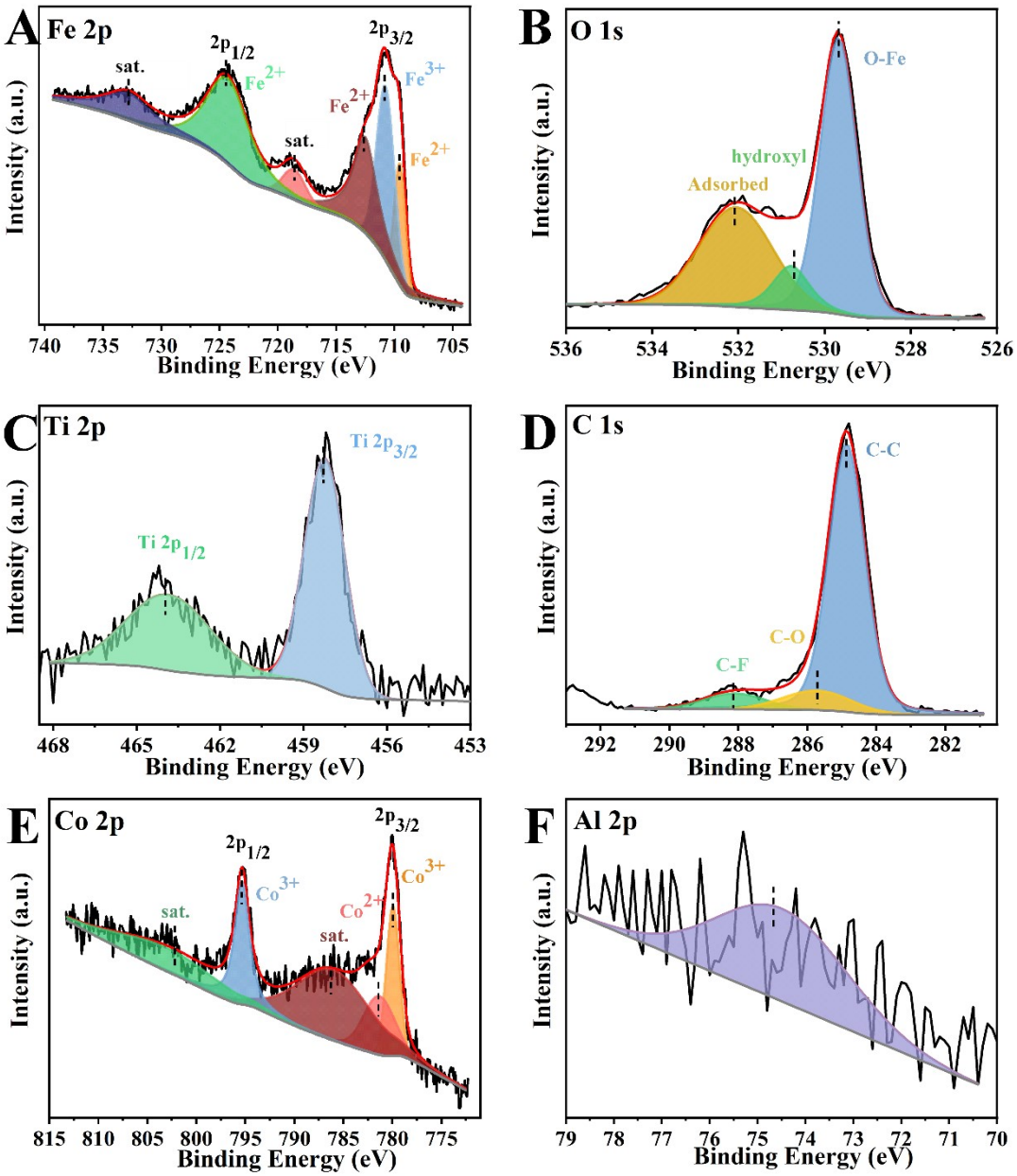

Figure S6. XPS spectra of Fe_2O_3-Ti_3C_2-CoAl photoanodes. (A) Fe 2p, (B) O 1s, (C) Ti 2p, (D) C 1s, (E) Co 2p, (F) Al 2p, respectively.

Additional discussion:

The surface chemical state and interaction in the prepared samples (Fe_2O_3-Ti_3C_2-CoAl) were surveyed by X-ray photoelectron spectroscopy (XPS) measurement. Figure S6 (B-F) show the XPS spectrum of O 1s, Fe 2p, Ti 2p, C 1s, Co 2p and Al 2p, respectively. In Figure S6F, no evident peaks of Al 2p could be detected, which should be resulted from the relatively low content of CoAl LDH cocatalyst. Thus, inductively coupled plasma (ICP) spectrometry was performed on the Fe_2O_3-Ti_3C_2-CoAl samples, and the obtained Al content is 2.45×10^{-3} mg/cm^2. This result can prove the

existence of Al element on the Fe_2O_3-Ti_3C_2-CoAl photoanodes.

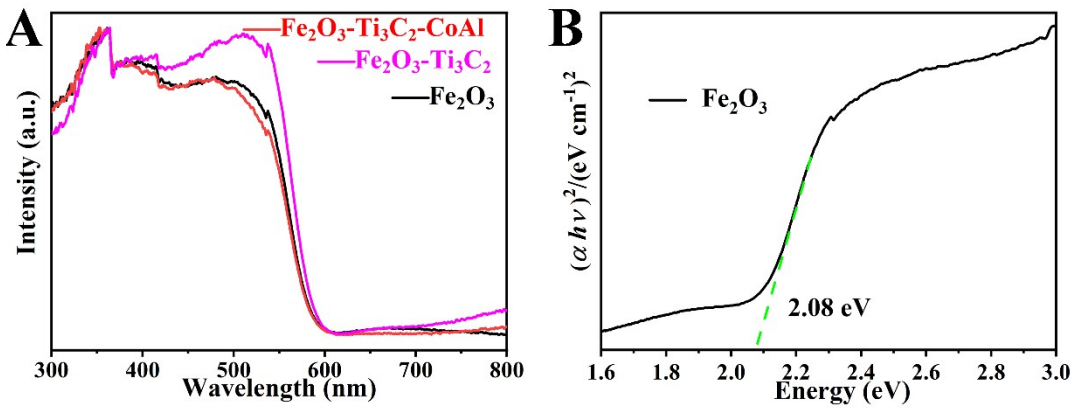

Figure S7. (A) UV-Vis diffuse reflectance spectra of Fe_2O_3, Fe_2O_3-Ti_3C_2 and Fe_2O_3-Ti_3C_2-CoAl, separately. (B) The $(\alpha h\nu)^2$ versus photon energy plots for Fe_2O_3.

Additional discussion:

Ultraviolet–visible (UV-vis) absorption (Figure S7) shows the similar spectral response range (≈ 600 nm) for the pristine Fe_2O_3, Fe_2O_3-Ti_3C_2 and Fe_2O_3-Ti_3C_2-CoAl photoanodes, and the pristine Fe_2O_3 photoanode exhibits a bandgap energy of 2.08 eV, which is consistent with recent reports.[4-5] After being modified with Ti_3C_2 and CoAl LDH, the absorption intensity of Fe_2O_3 remain almost unchanged, which proves that the Ti_3C_2 and CoAl LDH have negligible effect on the optical absorption property of dendritic Fe_2O_3.

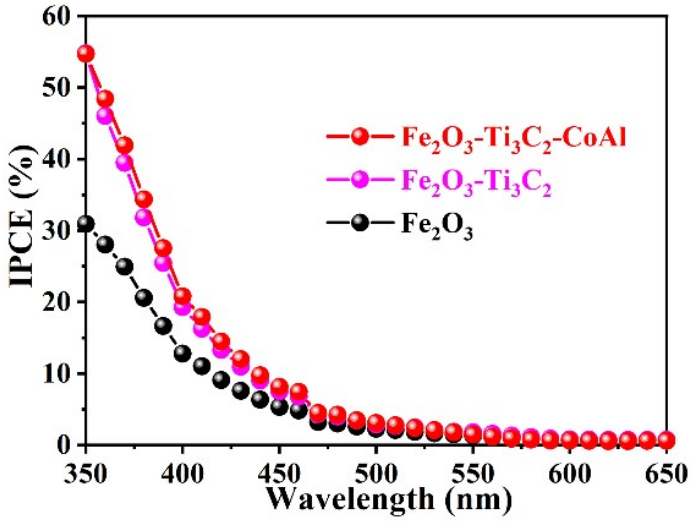

Figure S8. IPCE of Fe_2O_3, Fe_2O_3-Ti_3C_2 and Fe_2O_3-Ti_3C_2-CoAl photoanodes.

Additional discussion:

The improved PEC performance was also proved by incident photo-to-electron conversion

efficiency (IPCE) (Figure S8). The IPCE values of Fe_2O_3-Ti_3C_2-CoAl photoanode reached a maximum 54.7 % IPCE value at a wavelength of 350 nm.

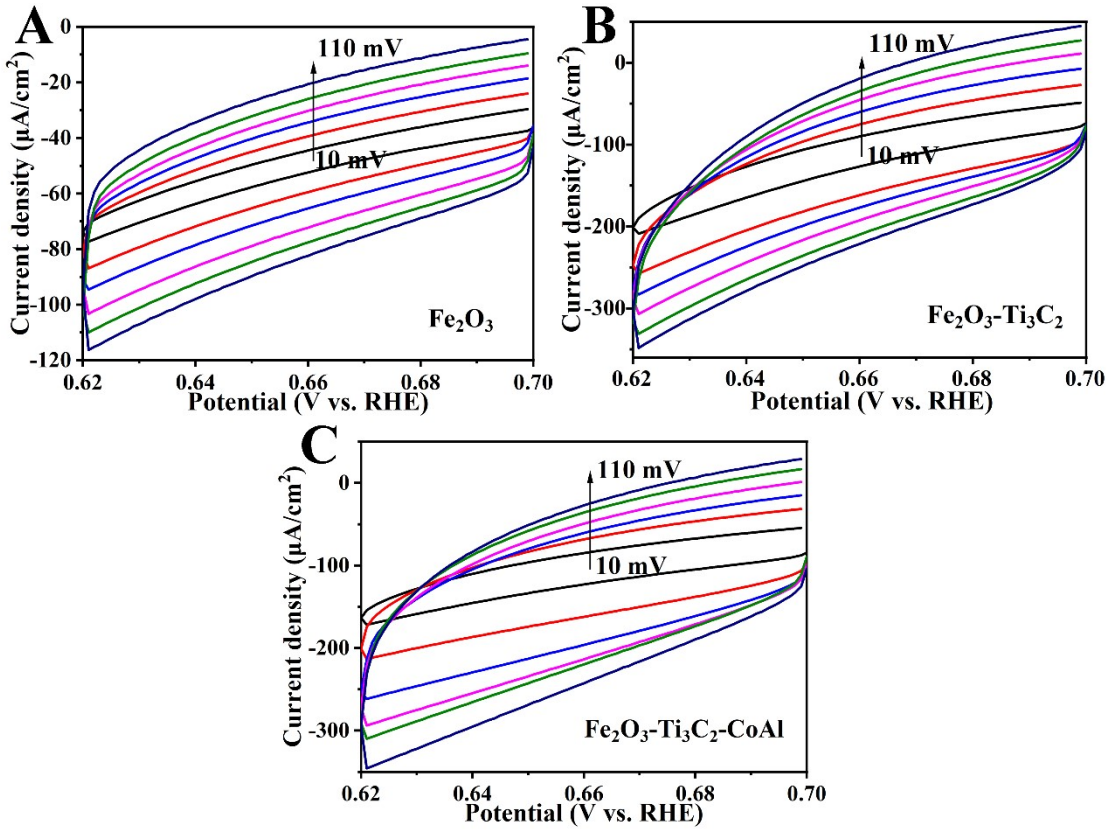

Figure S9. Electrochemical surface areas (ESCAs) tests towards OER in 1 M KOH. CV curves of (A) Fe_2O_3, (B) Fe_2O_3-Ti_3C_2, (C) Fe_2O_3-Ti_3C_2-CoAl photoanodes with different scanning rates.

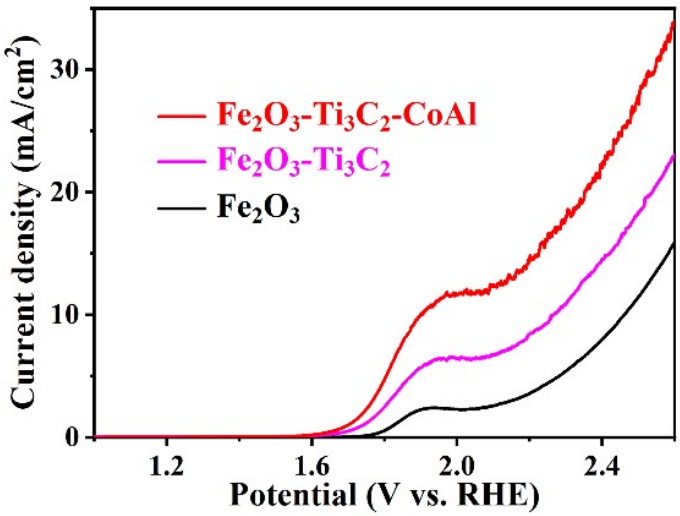

Figure S10. Electrochemical OER performance of Fe_2O_3, Fe_2O_3-Ti_3C_2 and Fe_2O_3-Ti_3C_2-CoAl photoanodes.

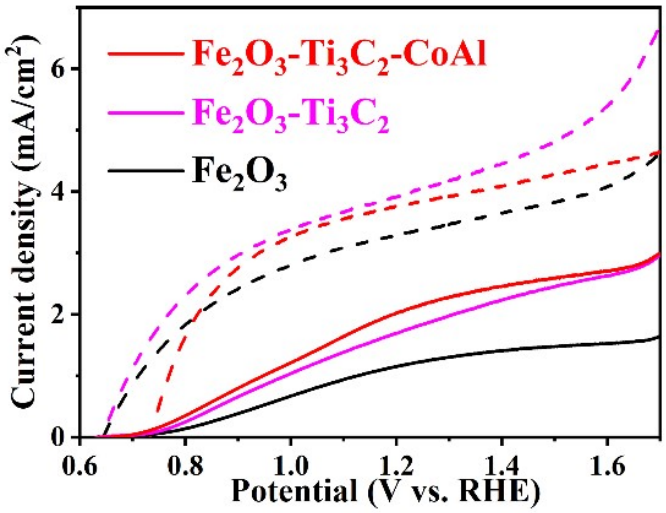

Fig S11. LSV curves of Fe_2O_3, Fe_2O_3-Ti_3C_2 and Fe_2O_3-Ti_3C_2-CoAl photoanodes for PEC H_2O (solid line) and H_2O_2 (dotted line) oxidation.

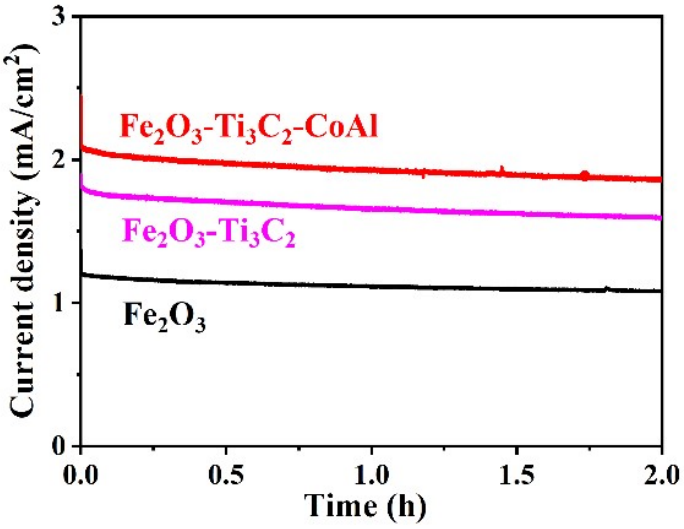

Figure S12. The long-term stability measurements were conducted in 1 M KOH at 1.23 V_{RHE} under AM 1.5G illumination.

Additional discussion:

Figure S12 shows the current-time curves of three photoanodes, illustrating the Fe_2O_3-Ti_3C_2-CoAl photoanode possesses excellent durability which retaining approximately 85 % of the initial photocurrent density with a steady photocurrent density of 1.78 mA cm^{-2} at 1.23 V_{RHE} during 2 h stability test. The 15% attenuation after 2 hours continuous test can be attributed to the partial oxidation of Ti_3C_2 due to the oxygen-rich environment and anodic potentials, and the Ti_3C_2 nanolayer could not be well protected by the CoAl layers.[6,7]

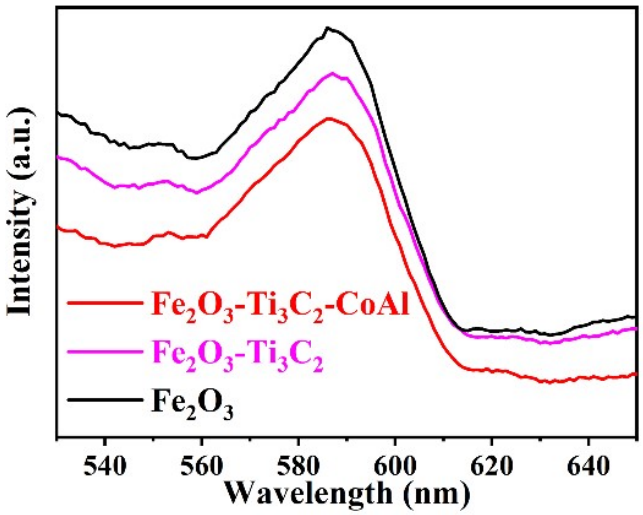

Figure S13. Photoluminescence spectra of the pristine Fe_2O_3, Fe_2O_3-Ti_3C_2 and Fe_2O_3-Ti_3C_2-CoAl photoanodes.

Additional discussion:

The results of photoluminescence (PL) spectroscopy were shown in Figure S13, which explore the recombination processes of photogenerated excitons.[8] The stronger the photoluminescence peak represents that the more electrons leave the conduction band and recombine with the hole, and the more photon energy is produced, indicating that the higher the recombination rate of electrons and holes, that is, the lower the separation efficiency. Obviously, the Fe_2O_3-Ti_3C_2-CoAl photoanode shows a much smaller PL intensity than both Fe_2O_3-Ti_3C_2 and Fe_2O_3 photoanodes, reflecting a higher charge separation efficiency.

Table S1. The values of the elements in equivalent circuit fitted in the Nyquist plots of Figure 3D.

Sample	R_s (Ω)	R_{ct1}	CPE1	R_{ct2} (Ω)	CPE2
Fe_2O_3	1.159	395.3	2.73×10^{-4}	2298.0	8.51×10^{-3}
Fe_2O_3-Ti_3C_2	1.411	3.312	9.86×10^{-6}	315.6	1.68×10^{-4}
Fe_2O_3-Ti_3C_2-CoAl	0.980	1.287	7.40×10^{-6}	313.7	8.1×10^{-4}

Reference:

[1] D. Yan, X. Fu, Z. Shang, J. Liu, H. Luo, *Chem. Eng. J.*, 2019, **361**, 853-861.

[2] Y. Jiang, T. Sun, X. Xie, W. Jiang, J. Li, B. Tian, C. Su, *Chemsuschem*, 2019, **12**, 1368-1373.

[3] Z. Zeng, Y. Yan, J. Chen, P. Zan, Q. Tian, P. Chen, *Adv. Funct. Mater.*, 2018, **29**, 1806500.

[4] C. Feng, S. Fu, W. Wang, Y. Zhang, Y. Bi, *App. Catal. B*, 2019, **257**, 117900.

[5] Y. Fu, Y. Lu, F. Ren, Z. Xing, J. Chen, P. Guo, W. Pong, C. Dong, L. Zhao, S. Shen, *Sol. RRL.*, 2020, **4**, 1900349.

[6] G. Yang, S. Li, X. Wang, B. Ding, Y. Li, H. Lin, D. Tang, X. Ren, Q. Wang, S. Luo, J. Ye, *Appl. Catal. B,* 2021, **297**, 120268.

[7] R. Ye, S. Sun, L. He, S. Yang, X. Liu, M. Li, P. Fang, J. Hu, *Appl. Catal. B,* 2021, **291**, 120107.

[8] C. Ye, J. Li, Z. Li, X. Li, X. Fan, L. Zhang, B. Chen, C. Tung, L. Wu, *ACS Catal.*, 2015, **5**, 6973-6979.